Epitaxial Self-assembly of Binary Molecular Components into Branched Nanowire Heterostructures for Photonic Applications

Qinghua Kong,[†,§] Qing Liao,*[‡] Zhenzhen Xu,[†,§] Xuedong Wang,[†,§] Jiannian Yao,[†] and Hongbing Fu*[†,‡,⊥]

[†]Beijing National Laboratory for Molecular Sciences (BNLMS), Institute of Chemistry, Chinese Academy of Sciences, Beijing 100190, People's Republic of China

[‡]Beijing Key Laboratory for Optical Materials and Photonic Devices, Department of Chemistry, Capital Normal University, Beijing 100048, People's Republic of China

[§]Graduate University of Chinese Academy of Sciences, Beijing 100049, People's Republic of China

[⊥]Collaborative Innovation Center of Chemical Science and Engineering, Tianjin 300072, People's Republic of China

S *Supporting Information*

ABSTRACT: We report a sequential epitaxial growth to prepare organic branched nanowire heterostructures (BNwHs) consisting of a microribbon trunk of 1,4-dimethoxy-2,5-di[4′-(cyano)styryl]benzene (COPV) with multiple nanowire branches of 2,4,5-triphenylimidazole (TPI) in a one-pot solution synthesis. The synthesis involves a seeded-growth process, where COPV microribbons are grown first as a trunk followed by a seeded-growth of TPI nanowire branches at the pregrown trunk surfaces. Selected area electron diffraction characterizations reveal that multiple hydrogen-bonding interactions between TPI and COPV components play an essential role in the epitaxial growth as a result of the structural matching between COPV and TPI crystals. A multichannel optical router was successfully realized on the basis of the passive waveguides of COPV green photoluminescence (PL) along TPI nanowire branches in a single organic BNwH.
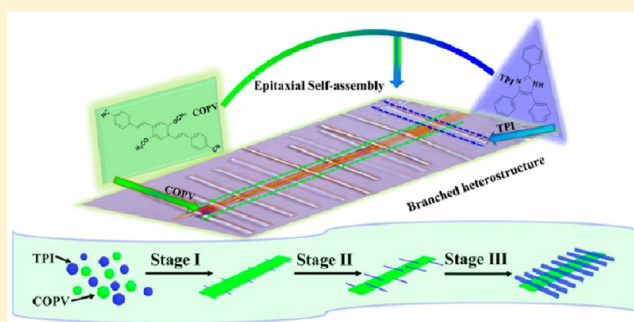
INTRODUCTION

One-dimensional (1D) semiconductor nanowires have been intensively investigated as promising building blocks for nanoscale optoelectronic devices, such as transistors,[1] lasers,[2] photodetectors,[3] and biosensors.[4] Recently, branched nanowire heterostructures (BNwHs), in which a number of secondary nanowires grow in the radial direction from the primary nanowire backbone, have attracted great attention,[5] because their 3D structure and large surface area naturally provide parallel connectivity and interconnection between nanowires for device integration. For example, dendritic BNwHs of ZnO have been demonstrated as highly ordered arrays of ultraviolet nanowire lasers.[5d] Also α-Fe$_2$O$_3$/SnO$_2$ BNwHs were used as anode materials of a lithium-ion battery, which exhibited superior electrochemical performance in comparison to those single-component nanowires.[5e] Consequently, various methodologies and mechanisms have been developed for fabrication of inorganic BNwHs, including sequential catalyst-assisted vapor−liquid−solid (VLS) growth,[6] vapor−solution combination growth,[7] and phase-induced branch growth,[5a] paving the way for encoding electronic and photonic functions at the branched junctions during the synthesis of BNwHs.[5f]

In recent years, the ever-increasing demands on high-speed optical communication and data processing have inspired great

efforts toward developing nanoscale optical components with the potential for use as high-speed data highways.[8] Organic semiconductors are promising candidates for such applications because of their broad spectral tunability, high optical cross sections, ease of structure tailoring as well as their ability to self-assemble for bottom-up fabrication.[9] In terms of fabrication, organic semiconductors are held together by noncovalent interactions, such as $\pi-\pi$ stacking, hydrogen bonding, and van der Waals interactions.[10] Single-component 1D organic nanostructures can be readily prepared based on $\pi-\pi$ stacking of conjugated molecules.[11] However, the controlled synthesis of organic BNwHs has met with limited successes.[12] In most cases, self-assembly of multiple molecular components driven by weak intermolecular interactions either generates a homogeneously mixed structure[13] or undergoes phase segregation leading to a process called orthogonal self-assembly.[13c,d]

In this study, we report a sequential epitaxial growth to prepare organic BNwHs consisting of a microribbon trunk of 1,4-dimethoxy-2,5-di[4′-(cyano)styryl]benzene (COPV, a green-emissive molecule, Figure 1A) with multiple nanowire
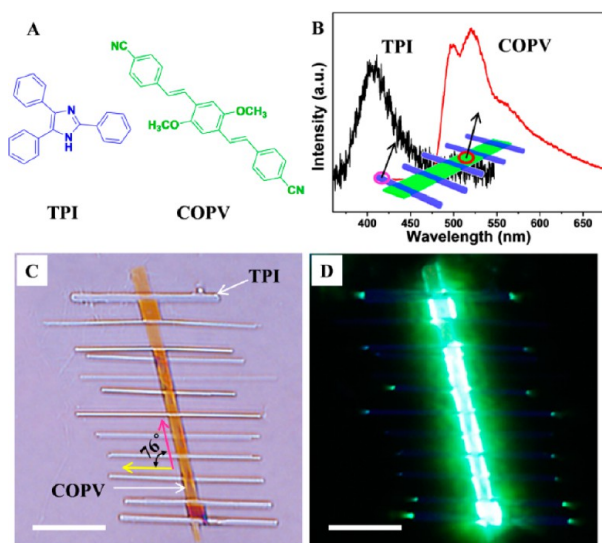
Figure 1. (A) Molecular structures of TPI and COPV. (B) Spatially resolved PL spectra recorded at the COPV microribbon trunk (red) and the TPI nanowire branch (black) positions. The excitation wavelengths for recording emission spectra of the COPV trunk and the TPI branch are 408 and 355 nm, respectively. (C) Bright-field optical micrograph and (D) the corresponding fluorescence micrograph of a typical organic BNwH excited by unfocused UV light (330–380 nm). All scale bars are 10 μm.

branches of 2,4,5-triphenylimidazole (TPI, a ultraviolet-emissive molecule, Figure 1A) in a one-pot solution synthesis. We found that COPV microribbons are formed first as a trunk unit; and then the surfaces of as-formed COPV trunk ribbons act as the nucleation template for heteroepitaxial growth of TPI nanowire branches. Selected area electron diffraction (SAED) characterizations reveal that multiple hydrogen-bonding interactions between TPI and COPV components play an essential role in the epitaxial growth as a result of the structural matching between COPV and TPI crystals. A multichannel optical router was successfully realized based on the passive waveguides of COPV green photoluminescence (PL) along TPI nanowire branches in a single organic BNwH.

RESULTS AND DISCUSSION

We prepared organic BNwHs using a modified reprecipitation method in a one-pot synthesis. First, a mixed stock solution containing both TPI (C_{TPI} = 1 mM) and COPV (C_{COPV} = 0.2 mM) in tetrahydrofuran (THF) was preprepared (the molar ratio between TPI and COPV, N_{TPI}: N_{COPV} = 5:1). To prepare BNwHs, 2 mL of hot water (75 °C) as a poor solvent was added dropwisely into 100 μL of the mixed stock solution (see Supporting Information). Figure 1C shows a typical bright-field optical microscopy image of as-prepared samples deposited on a quartz plate. It can be seen that organic BNwHs have been successfully prepared (also see Figure 6). The trunk of BNwH is microribbon with a length of 20–40 μm and a width of 2 ± 0.5 μm. The diameters of nanowire branches range from 700 to 1100 nm, and their lengths are 20–25 μm. Interestingly, the branch nanowires are parallel to each other, are evenly distributed along the trunk ribbon with a regular periodicity of 2–3 μm, and are an angle of 76° to the length direction of the trunk ribbon. Figure 1D displays a fluorescence microscopy image of the same BNwH as shown in Figure 1C, excited with unfocused UV light (330–380 nm). Remarkably, the trunk

ribbons and the branch nanowires emit light in different colors: the former exhibit white-greenish photoluminescence (PL) corresponding to COPV, whereas the latter present blueish PL corresponding to TPI. In addition, we also prepared single-component structures of TPI and COPV. It can be seen that the TPI nanowires emitted blue light, and COPV microribbons emitted green light were obtained (Supporting Information Figure S1). These results suggest that the trunk ribbon is composed of COPV components, whereas the branch nanowires are made by TPI molecules.

We further recorded spatially resolved PL spectra using a homemade confocal fluorescence microscopy (see Supporting Information Scheme S1). The excitation laser beams at different wavelengths were focused down to the diffraction limit with a spot size around 2 μm at different positions on a single BNwH (see the middle scheme in Figure 1B). And spatially resolved PL spectra were collected underneath using another 3D-movable objective coupled to an optical fiber and detected using a liquid nitrogen cooled charge-coupled device (CCD). The black and red curves in Figure 1B display the spatially resolved microarea PL spectra recorded in a transmission mode at the branch and the trunk positions. It is known that COPV molecules form J-aggregates in the solid state, which exhibits 0–0 and 0–1 emission bands at 491 and 518 nm (Supporting Information Figure S2), respectively, with a high fluorescence quantum yield (ϕ = 0.42 ± 0.5).[14] The PL spectrum recorded at the trunk position (red curve, excited with a 408 nm laser) resembles that of COPV nanoparticles, with a 0–0 band weaker than the 0–1 band probably due to the self-absorption effect, because COPV J-aggregates exhibit a small Stokes shift of 380 cm^{-1}.[14] Furthermore, we also selectively excited the branch nanowires with a 355 nm laser. As we expected, the PL spectrum recorded at the position of branch nanowires presents a single peak at 405 nm (black curve), which is consistent with that of TPI nanowires.[15]

Further structural analysis of organic BNwHs was carried out using transmission electron microscopy (TEM) and selected area electron diffraction (SAED) measurements. Figure 2A shows a typical TEM image of a single BNwH, revealing that the trunk and branches both have regular morphologies and smooth surfaces. The SAED pattern in Figure 2B, recorder for the microribbon trunk, could be identified and indexed to monoclinic COPV crystal (CCDC No. 838078) with cell parameters of a = 8.5110 (15) Å, b = 14.954 (3) Å, c = 8.4748 (15) Å, $\alpha = \gamma = 90°$, and $\beta = 104.292°$. The squared and circled sets of spots in Figure 2B are due to (002) and (−100) Bragg reflections with lattice spacing (d) values of $d_{(002),COPV}$ = 4.2 Å and $d_{(100),COPV}$ = 8.5 Å, respectively. Correlation of the orientation of the microribbon trunk in Figure 2A to the SAED pattern in Figure 2B suggests that single-crystalline microribbon trunk of COPV is grown preferentially along the $[001]_{COPV}$ direction, that is, the crystal c axis (also see Supporting Information Figure S3). Therefore, the microribbon trunk of COPV is bound by $(100)_{COPV}$ crystal facets on the side surfaces and by $(010)_{COPV}$ crystal facets on the top and bottom surfaces. Figure 2C presents the SAED pattern recorded for a branch nanowire crystal, which could be perfectly indexed to monoclinic TPI crystal (CCDC No. 720571), with lattice constants of a = 30.458 (5) Å, b = 11.828 (2) Å, c = 8.9033 (10) Å, $\alpha = \gamma = 90°$, and $\beta = 97.836°$. The squared and circled sets of diffraction spots in Figure 2C are due to (002) and (100) crystal planes with a lattice spacing of $d_{(002),TPI}$ = 4.5 Å and $d_{(100),TPI}$ = 30.4 Å, respectively. This clarifies that TPI
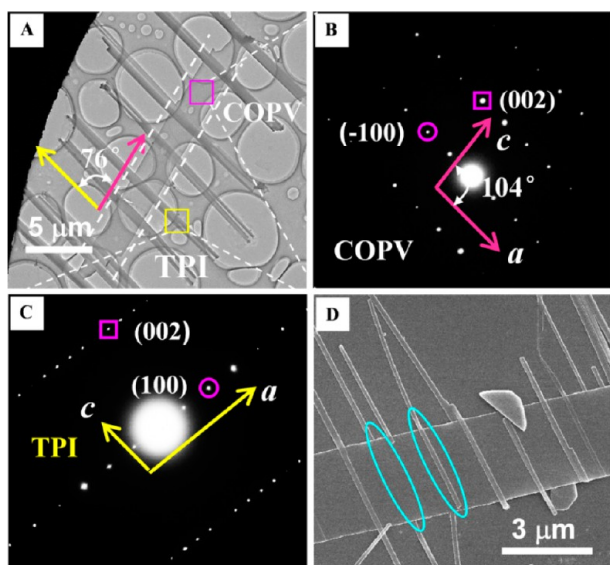
Figure 2. (A) A typical TEM image of a single BNwH. (B) SAED pattern of the COPV trunk recorded at the selected area marked by purple square in panel A. (C) SAED pattern of the TPI branch measured at the selected area marked by yellow square in panel A. (D) SEM image of a single BNwH formed at the early growth stage.

branch nanowires are also single crystals preferentially grown along the $[001]_{TPI}$ direction (the crystal c axis) (also see Supporting Information Figure S4). Also, this preferential growth along the $[001]_{TPI}$ direction leaves TPI nanowires bound by $(100)_{TPI}$ crystal facets on the side surfaces and by $(010)_{TPI}$ crystal facets on the top and bottom surfaces.

Different from the SAED technique that measures crystal planes perpendicular to the supporting substrate, X-ray diffraction (XRD) measures crystal planes parallel to the supporting substrate. Indeed, the XRD pattern of BNwHs filtered on the surface of an AAO membrane only shows the (110) peak of TPI together with the (020) peak of COPV, in good agreement with SAED results (Supporting Information Figure S5).

Combining the SAED and XRD results with the crystal structures of COPV and TPI, we could construct a molecular organization model at the junction region (Figure 3A). As mentioned above, the angle between the nanowire branches of TPI and the trunk ribbon of COPV in BNwHs (Figure 2A) is ca. 76°, which is factually supplementary to $\beta_{COPV} \approx 104°$ of COPV crystal, that is, the angle between the a and the c axes of

the monoclinic COPV crystal (Figure 2B and 3A). This means that the $[001]_{TPI}$ growth direction of TPI nanowires (the c_{TPI} axis in Figure 3A) is parallel to the $[100]_{COPV}$ direction of COPV microribbon (the a_{COPV} axis in Figure 3A), that is, $[001]_{TPI}//[100]_{COPV}$. It is widely accepted that lattice match is important for the epitaxial growth of heterostructures.[5a] In our case, there is only a small mismatch between $d_{(001),TPI} = 8.9$ Å and $d_{(100),COPV} = 8.5$ Å. This suggests that epitaxial growth of TPI branches along COPV trunk with an interfacial orientation relationship of $[001]_{TPI}//[100]_{COPV}$ is very possible. On the basis of the molecular packing structures of TPI and COPV single crystals, one could find that two parallel chains of TPI molecules interdigitated with each other stack along the $[001]_{TPI}$ direction via hydrogen bonding ($\cdots N \cdots H \cdots N \cdots$) in the nanowire branch (also see Supporting Information Figure S4); on the other hand, COPV molecules are stacked along the $[001]_{COPV}$ direction via $\pi-\pi$ stacking and hydrogen-bonding interactions in the trunk ribbon (also see Supporting Information Figure S3). Importantly, the distance between two hydrogen-bonding chains of TPI molecules (indicated as $d_{H,TPI}$ between two pink dashed lines in Figure 3B) is approximately 8.4 Å, equal to the value of $d_{(001),COPV}$ (indicated between two pink solid lines in Figure 3B), which is factually the distance between two cyano nitrogen atoms of neighboring COPV molecules (Figure 3B). This paves the way for the formation of hydrogen bonds between imidazole $-NH$ groups of TPI and cyano nitrogen atoms of COPV (i.e., TPI$-NH\cdots NC-$COPV) as marked within the white ellipse in Figure 3B. As a matter of fact, $d_{H,TPI} \approx d_{(001),COPV}$ and $d_{(001),TPI} \approx d_{(100),COPV}$ allow quadruple hydrogen-bonding interactions, which are driving forces for the epitaxial growth of TPI nanowire branches along the microribbon trunk of COPV.

Returning to Figure 2D, which displays a characteristic scanning electron microscopy (SEM) image of an individual BNwH, one could find that nanowires branches of TPI grow on both top and bottom surfaces of the trunk microribbon of COPV. This indicates that the COPV microribbon formed first and then acted as the nucleation template for the epitaxial growth of TPI nanowires. In order to have a closer inspection of the formation process of BNwHs, temporal morphology evolution was investigated by monitoring the samples obtained at different reaction-time intervals after injection of 2 mL of hot water (75 °C) into 100 μL of the mixed stock solution. Figure 4A$-$C shows the bright-field optical microscopy images of BNwHs obtained at 2, 5, and 10 min, respectively (also see Supporting Information Figure S6), with Figure 4D$-$F the corresponding fluorescence microscopy images. At the early stage, about 2 min after the injection (Figure 4A and 4D, Supporting Information Figure S6A), COPV microribbon was already observed; furthermore, selective nucleation of some TPI dots was also found at the edges of the trunk ribbon. Upon increasing the reaction time to 5 min (Figure 4B and E and Supporting Information Figure S6B), short rod-like structures, which are parallel to each other, have formed sticking out of one side of the trunk ribbon. When the reaction time exceeded 10 min (Figure 4C and F and Supporting Information Figure S6C), nanowire branches of TPI grew through the trunk ribbon of COPV with their lengths distributed evenly on both sides of the trunk. Meanwhile, the density of individual nanowires of TPI was found to decrease from Figure 4A to 4C with increasing the reaction time.

On the basis of the above observations, we propose a simple three-stage growth model, as illustrated in Figure 4G. After the
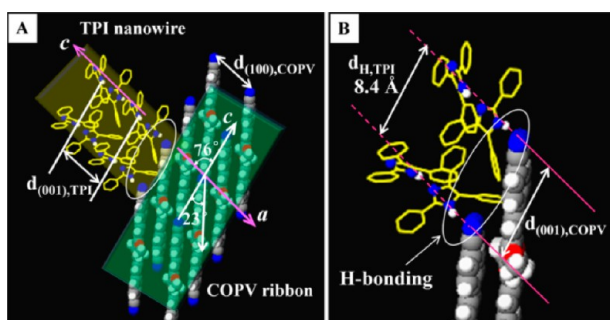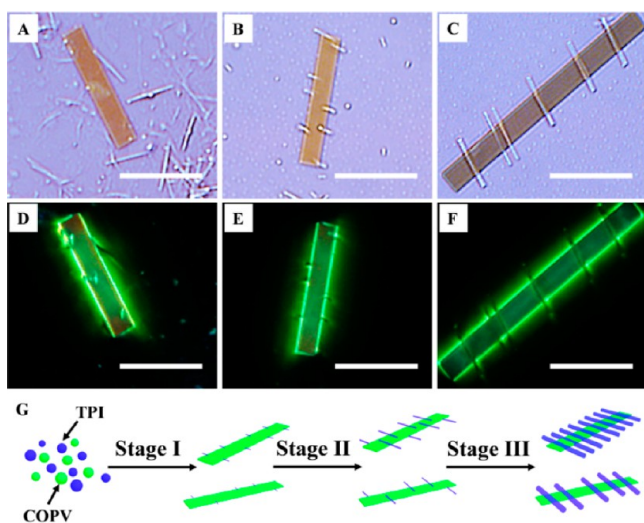

Figure 3. (A) Molecular packing arrangements of TPI molecules and COPV molecules at the junction region. (B) High-magnification of the junction region marked by the white ellipse in panel A.

Figure 4. Growth process of the BNwHs. Bright-field images (A–C) and the corresponding PL microscopy images (D–F) of BNwHs obtained at different reaction intervals: 2 min (A and D), 5 min (B and E), and 10 min (C and F), respectively. It is noted that Figure 4A–C (or 4D–F) are not for the same BNwH at different reaction intervals; instead, they depict typical shape evolution of ensemble BNwHs as a function of reaction time. All scale bars are 10 μm. (G) Schematic illustration of the growth process of the BNwHs.

injection, diffusion of water into the THF stock solution changes the solvent surroundings and induces the nucleation process through which self-assembly starts to take place. It can be clearly seen that COPV microribbons are formed in stage I. We found that the formation of pure COPV clusters in THF exhibits a threshold concentration of 1.8×10^{-5} M, much lower than that (5.0×10^{-5} M) for the formation of pure TPI clusters in THF (see Supporting Information Figure S7).[15] When the water was dropped into the mixed stock solution, the lower aggregation threshold concentration of COPV may speed up the nucleation rate of COPV molecules. Moreover, in our case, TPI has a stronger affinity to water than COPV because the polarity of TPI is larger than that of COPV. This also makes the aggregation rate of TPI slower than that of COPV.[16] Upon increasing the reaction time, the temperature decreases, reaching the nucleation threshold of TPI. Most importantly, those previously formed COPV microribbons (in Stage I) are capable of serving as a template for the heterogeneous nucleation of TPI molecules on their surfaces through multiple hydrogen bonds, that is, TPI−NH···NC−COPV (Figure 3B) during Stage II. Finally, the epitaxial growth of TPI along the $[100]_{COPV}$ direction followed by 1D-elongation along the $[001]_{TPI}$ direction leads to perfect BNwHs consisting of COPV trunk ribbon with uniform TPI nanowire branches (Stage III).

According to the formation mechanism and growth process discussed above, the branched heterostructures can be finely tuned by changing the concentration of COPV and TPI solution. From bright-field optical micrographs (Supporting Information Figure S8) and the PL images of the as-prepared samples excited by unfocused UV light (Figure 5), it is noted that different heterostructures were obtained when the concentration of COPV and TPI solution were varied. (i) If C_{TPI} was fixed at 1 mM, a decrease of C_{COPV} to 0.05 mM leads to BNwHs consisting of narrow COPV ribbons and short TPI branches, as shown in Figure 5A. In contrast, doping of COPV components in TPI branches of BNwHs and some pure COPV
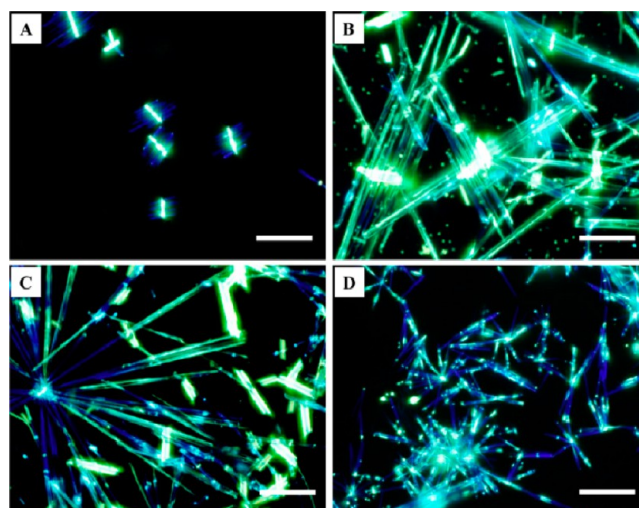

Figure 5. Fluorescence micrographs of BNwHs prepared at four different concentration ratios of TPI to COPV: (A) 1:0.05, (B) 1:0.5, (C) 0.5:0.2, and (D) 3:0.2. All scale bars are 20 μm.

ribbons were found when the C_{COPV} was increased to 0.5 mM (Figure 5B), suggesting that COPV molecules are overloaded under this condition. (ii) On the other hand, if C_{COPV} was fixed at 0.2 mM, a decrease of C_{TPI} to 0.5 mM results in many pure COPV ribbons and some TPI nanowires doped with COPV dots (Figure 5C). Under this condition, we speculate that COPV microribbons were formed first, and the formation of TPI nanowires were delayed, probably because a decrease of C_{TPI} to 0.5 mM could lead to a much slower aggregation rate of TPI components than that of COPV molecules and, therefore, phase segregation between them. Remarkably, when the C_{TPI} was increased to 3 mM (Figure 5D), shorter TPI branches doped by COPV components are observed and BNwHs are almost missing. Under this condition, TPI could be nucleated first due to high concentration and then the COPV molecules aggregated together with the TPI rod resulted in the doped structures, similar to the case of organic heterostructures composed of TPI and 9,10-bis (phenylethynyl) anthracene.[17] Therefore, during the assembly process of BNwHs, Stage I is the key stage which can be adjusted by the concentrations of these two components. Meanwhile, by varying the preparation temperature, we can obtain BNwHs consisting of TPI branches and COPV trunks with different lengths and widths (Figure 6). This indicates that the temperature of water has an impact on the second and third stage of the growth. Especially, the nuclei number density increases with decreasing the temperature.[18] Accordingly, the sizes of BNwHs would become smaller with decreasing the temperature as a result of the increased number density of nuclei (i.e., the number of BNwHs) when the total
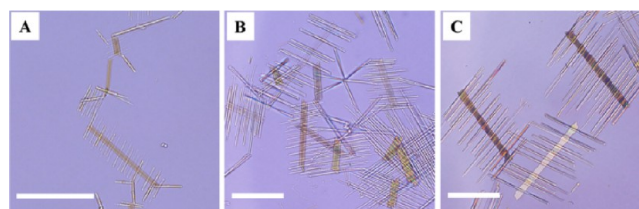

Figure 6. Bright-field optical micrographs of BNwHs obtained at different temperatures: (A) 30 °C, (B) 55 °C, and (C) 75 °C. All scale bars are 10 μm.

amount of growth units of both TPI and COPV is kept constant.

This unique branched heterostructure exhibits optical channeling properties.[19] Figure 7A shows a single typical
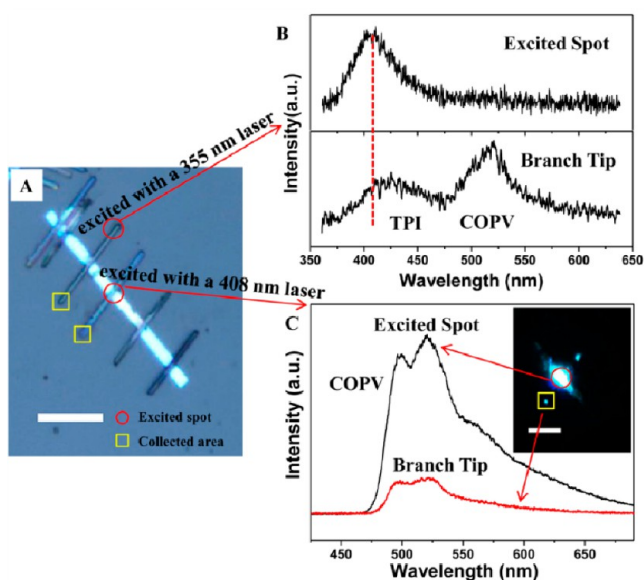

Figure 7. (A) Bright-field optical micrograph of a single BNwH. (B) Spatially resolved PL spectra of the branch recorded at the excited spot (red circle) and branch tip region (yellow square) excited by a 355 nm laser marked in panel A. (C) Spatially resolved PL spectra of the trunk recorded at the excited spot (red circle) and branch tip region (yellow square) excited by a 408 nm laser marked in panel A. The inset shows the corresponding PL image. All scale bars are 10 μm.

BNwH used for the photonic characterization, which consists of six TPI branches grown on a single COPV trunk with an average spacing of ~5 μm. We recorded spatially resolved microarea PL spectra of a typical single BNwH excited at two different laser wavelengths. When the branch was excited by a 355 nm laser, the PL spectrum taken locally from the excited spot (red circle) presents a single peak at 405 nm (Figure 7B, top curve), which is consistent with that of TPI nanowires. Interestingly, the PL spectrum recorded at another tip of the branch (yellow square) exhibits not only the TPI peak at 425 nm that is red-shifted from 405 nm but also an additional peak at 518 nm due to the COPV component (Figure 7B, bottom curve). When the branch tip was excited with an input laser signal, the emitted blue light propagates toward its distal end. The blue light is out-coupled to the distal end via two processes. The first is photon reabsorption, in which the TPI emission guided in the branch may be scattered at the junctions and injected into the COPV trunk, causing the absorption of TPI PL by COPV components along the trunk cavities, as proved by the spectral overlap shown in Supporting Information Figure S2. As a result, the PL of TPI is partially quenched, and the green emission of COPV is guided toward the tip of TPI branch. The second is self-absorption of TPI branch, which is assumed to induce a red shift of the PL spectrum of TPI.

On the other hand, the bright tip of branch was observed when the trunk was excited by a 408 nm laser with a spot size of 4−5 μm (inset of Figure 7C). At this point, one can recall the PL image illustrated in Figure 1D, which verifies the green emission output from each tip of nanowire branches when the

as-prepared BNwH was excited with unfocused UV light. Indeed, the microarea PL spectra (Figure 7C) of the trunk recorded at the excited spot and the branch tip both show 0−0 and 0−1 emission bands at 491 and 518 nm due to the characteristic PL of COPV component. Clearly, efficient passive waveguiding behavior is observed in our organic BNwHs.[20] Meanwhile, we found only the tips of branches connected to the excited spot are bright and the other branches' tips are dark (inset of Figure 7C), which indicates that the green light emitted by COPV propagates only along the trunk width and then was out-coupled into the TPI branch to propagate toward the branch tip. Therefore, we can modulate the multichannel passive waveguide via varying the size of the excitation laser beam. Recently, Takazawa and co-workers investigated the active waveguiding in J-aggregates of thiacyanine nanofibres due to propagation of exciton polaritons (EPs) formed by strong coupling between the excitons and the laser-induced fluorescence.[21] In our case, COPV molecules also form J-aggregates in microribbon trunks. Previous studies have shown that the coherence length of Frenkel excitons in COPV J-aggregates is estimated to be about 2−3 moelcules,[14] smaller than that of Wannier-Mott excitons in a single quantum wire of polydiacetylene chain.[22] Nevertheless, the large oscillator strength of COPV J-aggregate facilitates the formation of EPs, which lead to a large group refractive index for waveguiding.[21] Moreover, TPI nanowires are epitaxially grown on the top and bottom surfaces of COPV trunk ribbon in BNwHs (see Figure 2D). Hence, the coupling of COPV PL from trunk to nanowire branch channels can be highly efficient. Such high-performance multichannel waveguides will provide useful information for designing miniaturized photonic circuits.

To demonstrate the utility of BNwHs in the context of photonic circuit, we constructed an optical router using a single BNwH, schematically shown in Figure 8A. We selectively excited COPV components of a single BNwH using a focused strip-beam (10 × 250 μm) from a 408 nm laser. Then, spatially
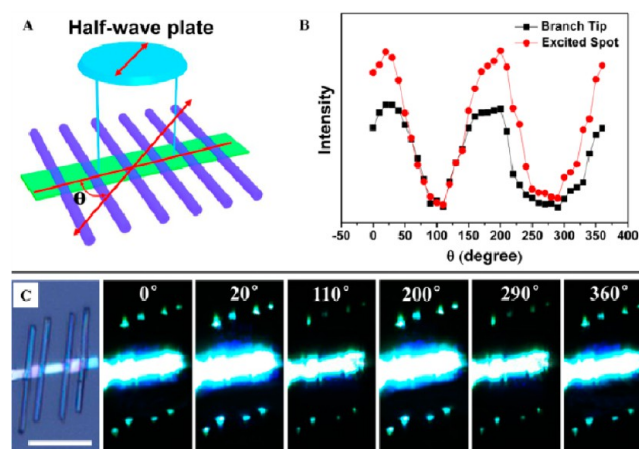

Figure 8. (A) Schematic illustration of the measurement setup for polarized excitation. The angle, θ, refers to the relative angle between the polarization of the excitation laser and the length direction of COPV trunk ribbon. The COPV microribbon was excited with a striped polarized laser beam and the modulated light signals were collected at excited spot and the tips of branches. (B) The variation of the emission intensity from COPV microribbon and the tips of branches as a function of polarization angle ($\theta = 0−360°$). (C) Bright-field optical image and PL images of the BNwHs taken by exciting the COPV ribbon at different polarization angles. The scale bar is 10 μm.

resolved microarea PL spectra were recorded at both the trunk and the tips of branch positions. The angle, θ, which is defined as the angle between the polarization of the excitation laser and the length direction of COPV trunk ribbon (Figure 8A), is systematically adjusted from 0 to 360° using a half-wave plate. Figure 8C shows the bright-field optical image and the PL images excited by a 408 nm laser of a typical single BNwH used for the photonic characterizations. The branches exhibited typical characteristics of passive optical waveguide with bright green emission of COPV at all tips, which are consistent with the results discussed in Figure 7. It can be seen from Figure 8B that integrated PL intensities recorded at both the trunk body and the branch tip positions oscillate with a period of 180°, between the maximum (I_{max}, as "1" or "ON" state) at θ = 20 or 200° and the minimum (I_{min}, as "0" or "OFF" state) at θ = 110 or 290° (Figure 8C). It is worth noting that the transition dipole moment of COPV molecules is along the molecular long axes,[23] which forms an angle of 23° to the length direction of COPV trunk ribbon (the crystal c axis) as illustrated in Figure 3A. Therefore, θ = 20 or 200° means that the input laser polarization is parallel to the transition dipole moment of COPV molecules, leading to the maximally emissive output from nanowire tip on "ON" state; in contrast, θ = 110 or 290° means that the input laser polarization is perpendicular to the transition dipole moment of COPV molecules, giving rise to the minimally emissive output from nanowire tips on "OFF" state. That is, the passive waveguides of COPV green PL along TPI nanowires can be efficiently modulated by controlling the incident laser polarization, making a BNwH perfectly a multichannel optical router. The on/off ratio $R = I_{max}/I_{min}$ was determined to be 12 and 9, yielding a polarization ratio $\rho = (R - 1)/(R + 1)$,[24] as high as 0.85 and 0.8 at the trunk body and the branch tip, respectively (Figure 8B), which are comparable and even higher than that of single crystalline CdSe nanorods (ρ = 0.7−0.86).[24]

CONCLUSION

In summary, organic BNwHs were synthesized in a large scale by a simple one-pot solution method. Temporal optical microscopy observations suggest that COPV microribbons are formed first as a trunk unit, and then the surfaces of as-formed COPV trunk ribbons act as the nucleation template for heteroepitaxial growth of TPI nanowire branches. We found that multiple hydrogen-bonding interactions between TPI and COPV components play an essential role in the epitaxial growth as a result of the crystallographic epitaxial relationship between the COPV trunk and the TPI branches. A multi-channel optical router was successfully realized based on the passive waveguide of COPV green PL along TPI nanowire branches with a single organic BNwH. This work opens opportunities for exploring the high-quality organic−organic heterostructures as well as their potential application in future photonics.

ASSOCIATED CONTENT

Ⓢ Supporting Information

Experimental details, bright-field images, PL images, the absorption and emission spectra. This material is available free of charge via the Internet at http://pubs.acs.org.

AUTHOR INFORMATION

Corresponding Authors

hongbing.fu@iccas.ac.cn.

liaoqing@cnu.edu.cn.

Notes

The authors declare no competing financial interest.

REFERENCES

(1) Xiang, J.; Lu, W.; Hu, Y. J.; Wu, Y.; Yan, H.; Lieber, C. M. *Nature* **2006**, *441*, 489.

(2) (a) Chu, S.; Wang, G. P.; Zhou, W. H.; Lin, Y. Q.; Chernyak, L.; Zhao, J. Z.; Kong, J. Y.; Li, L.; Ren, J. J.; Liu, J. L. *Nat. Nanotechnol.* **2011**, *6*, 506. (b) Xu, Z. Z.; Liao, Q.; Shi, Q.; Zhang, H. L.; Yao, J. N.; Fu, H. B. *Adv. Mater.* **2012**, *24*, OP216.

(3) Wang, J. F.; Gudiksen, M. S.; Duan, X. F.; Cui, Y.; Lieber, C. M. *Science* **2001**, *293*, 1455.

(4) (a) Cui, Y.; Lieber, C. M. *Science* **2001**, *291*, 851. (b) Patolsky, F.; Lieber, C. M. *Mater. Today* **2005**, *8*, 20.

(5) (a) Manna, L.; Milliron, D. J.; Meisel, A.; Scher, E. C.; Alivisatos, A. P. *Nat. Mater.* **2003**, *2*, 382. (b) Meng, G. W.; Han, F. M.; Zhao, X. L.; Chen, B. S.; Yang, D.; Liu, J. X.; Xu, Q. L.; Kong, M. G.; Zhu, X. G.; Jung, Y. J.; Yang, Y. J.; Chu, Z. Q.; Ye, M.; Kar, S.; Vajtai, R.; Ajayan, P. M. *Angew. Chem., Int. Ed.* **2009**, *48*, 7166. (c) Lim, B.; Xia, Y. N. *Angew. Chem., Int. Ed.* **2011**, *50*, 76. (d) Yan, H. Q.; He, R. R.; Johnson, J.; Law, M.; Saykally, R. J.; Yang, P. D. *J. Am. Chem. Soc.* **2003**, *125*, 4728. (e) Zhou, W. W.; Cheng, C. W.; Liu, J. P.; Tay, Y. Y.; Jiang, J.; Jia, X. T.; Zhang, J. X.; Gong, H.; Hng, H. H.; Yu, T.; Fan, H. J. *Adv. Funct. Mater.* **2011**, *21*, 2439. (f) Jiang, X. C.; Tian, B. Z.; Xiang, J.; Qian, F.; Zheng, G. F.; Wang, H. T.; Mai, L. Q.; Lieber, C. M. *Proc. Natl. Acad. Sci. U.S.A.* **2011**, *108*, 12212.

(6) Wang, D. L.; Qian, F.; Yang, C.; Zhong, Z. H.; Lieber, C. M. *Nano Lett.* **2004**, *4*, 871.

(7) Cheng, C. W.; Liu, B.; Yang, H. Y.; Zhou, W. W.; Sun, L.; Chen, R.; Yu, S. F.; Zhang, J. X.; Gong, H.; Sun, H. D.; Fan, H. J. *ACS Nano* **2009**, *3*, 3069.

(8) Clark, J.; Lanzani, G. *Nat. Photonics* **2010**, *4*, 438.

(9) Chénais, S.; Forget, S. *Polym. Int.* **2012**, *61*, 390.

(10) Hoeben, F. J. M.; Jonkheijm, P.; Meijer, E. W.; Schenning, A. P. H. J. *Chem. Rev.* **2005**, *105*, 1491.

(11) (a) Moon, H.; Zeis, R.; Borkent, E.-J.; Besnard, C.; Lovinger, A. J.; Siegrist, T.; Kloc, C.; Bao, Z. N. *J. Am. Chem. Soc.* **2004**, *126*, 15322. (b) Zang, L.; Che, Y. K.; Moore, J. S. *Acc. Chem. Res.* **2008**, *41*, 1596. (c) Zhao, Y. S.; Fu, H. B.; Peng, A. D.; Ma, Y.; Liao, Q.; Yao, J. N. *Acc. Chem. Res.* **2009**, *43*, 409. (d) Briseno, A. L.; Mannsfeld, S. C. B.; Jenekhe, S. A.; Bao, Z. N.; Xia, Y. N. *Mater. Today* **2008**, *11*, 38.

(12) (a) Zheng, J. Y.; Yan, Y. L.; Wang, X. P.; Zhao, Y. S.; Huang, J. X.; Yao, J. N. *J. Am. Chem. Soc.* **2012**, *134*, 2880. (b) Bu, L.; Pentzer, E.; Bokel, F. A.; Emrick, T.; Hayward, R. C. *ACS Nano* **2012**, *6*, 10924.

(13) (a) Vijayakumar, C.; Praveen, V. K.; Ajayaghosh, A. *Adv. Mater.* **2009**, *21*, 2059. (b) Abbel, R.; Grenier, C.; Pouderoijen, M. J.; Stouwdam, J. W.; Leclère, P. E. L. G.; Sijbesma, R. P.; Meijer, E. W.; Schenning, A. P. H. J. *J. Am. Chem. Soc.* **2008**, *131*, 833. (c) Jonkheijm, P.; Stutzmann, N.; Chen, Z.; de Leeuw, D. M.; Meijer, E. W.; Schenning, A. P. H. J.; Würthner, F. *J. Am. Chem. Soc.* **2006**, *128*, 9535. (d) Brizard, A.; Stuart, M.; van Bommel, K.; Friggeri, A.; de Jong, M.; van Esch, J. *Angew. Chem., Int. Ed.* **2008**, *47*, 2063.

(14) Xu, Z. Z.; Liao, Q.; Wu, Y. S.; Ren, W. L.; Li, W.; Liu, L. B.; Wang, S.; Gu, Z. J.; Zhang, H. L.; Fu, H. B. *J. Mater. Chem.* **2012**, *22*, 17737.

(15) Liao, Q.; Fu, H. B.; Wang, C.; Yao, J. N. *Angew. Chem.* **2011**, *123*, 5044.

2387

dx.doi.org/10.1021/ja410069k | *J. Am. Chem. Soc.* 2014, 136, 2382−2388

(16) Nakashima, H.; Fujiki, M.; Koe, J. R.; Motonaga, M. *J. Am. Chem. Soc.* **2001**, *123*, 1963.

(17) Zhang, C.; Yan, Y. L.; Jing, Y.-Y.; Shi, Q.; Zhao, Y. S.; Yao, J. N. *Adv. Mater.* **2012**, *24*, 1703.

(18) Wei, L.; Yao, J. N.; Fu, H. B. *ACS Nano* **2013**, *7*, 7573.

(19) Sirbuly, D. J.; Law, M.; Pauzauskie, P.; Yan, H.; Maslov, A. V.; Knutsen, K.; Ning, C.-Z.; Saykally, R. J.; Yang, P. D. *Proc. Natl. Acad. Sci. U.S.A.* **2005**, *102*, 7800.

(20) Chandrasekhar, N.; Chandrasekar, R. *Angew. Chem., Int. Ed.* **2012**, *51*, 3556.

(21) (a) Takazawa, K.; Inoue, J.-i.; Mitsuishi, K.; Kuroda, T. *Adv. Funct. Mater.* **2013**, *23*, 839. (b) Takazawa, K.; Inoue, J.-i.; Mitsuishi, K.; Takamasu, T. *Phys. Rev. Lett.* **2010**, *105*, 067401.

(22) (a) Yamagata, H.; Spano, F. C. *J. Chem. Phys.* **2011**, *135*, 054906. (b) Dubin, F.; Melet, R.; Barisien, T.; Grousson, R.; Legrand, L.; Schott, M.; Voliotis, V. *Nature Physics* **2005**, *2*, 32.

(23) Spano, F. C. *Annu. Rev. Phys. Chem.* **2006**, *57*, 217.

(24) Hu, J. T.; Li, L.-s.; Yang, W. D.; Manna, L.; Wang, L.-w.; Alivisatos, A. P. *Science* **2001**, *292*, 2060.